

The red supergiants & Wolf-Rayet stars of NGC 604

John J. Eldridge¹ * & Mónica Relaño¹ †

¹*Institute of Astronomy, The Observatories, University of Cambridge, Madingley Road, Cambridge, CB3 0HA*

24 September 2018

ABSTRACT

We study the post-main sequence stars in NGC 604, the most luminous HII region in M33. Previously, a number of Wolf-Rayet (WR) stars and one red supergiant (RSG) have been discovered. Based on broadband photometry of the region, we present evidence that is consistent with the presence of this RSG and with three more RSG candidates. Using SED fitting based on HST UVIJHK photometry we estimate the ages of the WR stars and RSGs finding that the two populations are from distinct formation episodes with ages 3.2 ± 1.0 Myrs and 12.4 ± 2.1 Myrs, respectively. The RSGs have greater extinctions towards their line of sight than the WR stars consistent with the RSGs producing large amount of dust. Using the WR and RSG populations and similar SED fits to the most massive O stars we estimate that the total stellar mass is $(3.8 \pm 0.6) \times 10^5 M_{\odot}$. We find a large discrepancy between the expected H α flux from such a massive cluster and that one observed. This suggests that 49^{+16}_{-19} percent of the ionizing photons produced by massive stars in NGC 604 is leaking from this HII region. We also suggest that the implications of an old RSG population mean that if NGC 604 was more distant and only observed in the infrared (IR) it would be difficult to study the youngest burst of star formation due to the contamination of RSGs.

Key words: stars: evolution – binaries: general – stars: Wolf-Rayet – stars: supergiants – HII regions: NGC 604 – galaxies: individual: M33

1 INTRODUCTION

NGC 604 is the most luminous and massive HII region in the nearby galaxy M33. Due to its large size, great mass and proximity it has been intensively studied to gain insight into the physics of HII regions and the evolution of massive stars (e.g. Hunter et al. 1996; Terlevich et al. 1996; Drissen et al. 1993, 2008; Maíz-Apellániz et al. 2004; González-Delgado & Pérez 2000, among others). Of paramount importance is to determine the age of the stellar population and the different stellar types present in this region, because a deeper knowledge of this object can help us to infer properties for star-forming regions of similar types in distant galaxies.

The confirmed stellar constituents of NGC 604 are OB stars, WR stars and at least one spectroscopically confirmed RSG (Hunter et al. 1996; Terlevich et al. 1996; Drissen et al. 2008). The different stellar types that NGC 604 harbours makes this HII region an ideal object to study its stellar population and to test stellar evolution and population synthesis models. NGC 604 is a key region to test whether the population inferred from *re-*

solved stellar populations can also match the *unresolved* spectral features that would be used in more distant galaxies. In this paper we use this region to qualitatively check the accuracy of the binary population and spectral synthesis (BPASS) code described in Eldridge & Stanway (2009) and at <http://www.bpass.org.uk>. Here we analyze the resolved stellar population observed with deep Hubble Space Telescope (HST) images and study the region as an unresolved object by using the integrated spectrum (González-Delgado & Pérez 2000) and observations of Relaño & Kennicutt (2009).

The possible presence of RSGs in NGC 604 comes from the spectroscopic evidence of Terlevich et al. (1996). Hunter et al. (1996) suggested the existence of a supergiant population based on HST stellar photometry, but these authors could not elaborate further these ideas since their observations were limited to the visible part of the spectrum. Recently, Barbá et al. (2009) have shown the complexity of the stellar population of this region using infrared NICMOS (Near Infrared Camera and Multi-Object Spectrometer) observations. They found evidence of massive young stellar object candidates and suggested the existence of a RSG population within the region.

Here we aim to study in detail the post-main sequence objects RSGs and WR stars of NGC 604, along with the

* E-mail: jj@ast.cam.ac.uk

† Email: mrelano@ast.cam.ac.uk

most massive main-sequence stars in the region. We obtain the photometry for the stars within NGC 604 in the IR-NICMOS filters and combine the results with the optical photometry performed by Hunter et al. (1996). We analyze the Spectral Energy Distribution (SED) of these stars from the optical to the IR wavelength range and investigate whether the RSG and WR populations have different ages. We then attempt to infer from these observations the total stellar mass and check if this is consistent with other observations such as the total H α flux from NGC 604.

2 EVIDENCE OF RED SUPERGIANTS IN NGC 604

The stellar content of NGC 604 was previously studied by Hunter et al. (1996) using UVI photometry. These authors showed the existence of numerous massive main-sequence stars and identified a candidate WR population in their colour-magnitude diagram (CMD). They also suggest the existence of numerous stars bright enough to be blue or red supergiants, which would indicate an older sub-population in NGC 604. Due to the limitation of their data, restricted only to the visible part of the spectrum, they did not study this cool and evolved stellar population. Taking advantage of the available NICMOS-IR data for this region and the comparison with the optical photometry, we now investigate further this evolved population. Using Hunter et al.'s photometry we selected stars in the central cluster of the region (Cluster A, as defined in Hunter et al. (1996)) with magnitudes and colours in the range of $F555W-F814W > 1$ and $F555W < -6$ and make a list of possible RSG candidates in NGC 604. These limits ensure we are taking massive ($M > 15 M_{\odot}$) RSGs and therefore we can compare this population with the massive WRs detected by Drissen et al. (2008).

2.1 NICMOS data analysis

NGC 604 was observed with the NICMOS (NIC2) on board the Hubble Space Telescope (HST) under the ID program 10419 (IP: R. Barbá) with the filters F110W, F160W and F205W (similar to J, H and K filters). We retrieved 6 fields from the HST Multimission Archive at the Space Telescope Institute (MAST), 5 covering the central part of NGC 604 and another covering an outside field for background subtraction. Each image has a field of view of 19.2×19.2 arcsec and a pixel scale of 0.075 arcsec.

The retrieved data were processed by the pipeline software Calnica (Version 4.4.0) but further analysis needed to be performed to obtain the final mosaic images. First we, masked out the Coronagraphic Hole and applied the MultiDrizzle software package¹ to create the final cosmic ray-free mosaic images. The retrieved F205W images showed some residuals due to a bad flat-field correction after being processed by Calnica with the default calibration files provided in the data archive. Therefore we generated a new flat-field using the F205W background images and reprocessed the images with it. The use of this flat-field clearly improved the final images for this filter. Finally, the ~ 20 rows of the

CCD affected by vignetting were eliminated from the images. We then created the mosaic image for the 5 fields in each filter using the World Coordinate System information from the headers. The final image for the F205W filter is shown in Fig. 1. The angular resolution (FWHM) in the final images are 0.16, 0.18, 0.20 arcsec for the corresponding filters F110W, F160W, F205W.

We obtained the stellar magnitudes for each filter using the crowded-field fitting software DAOPHOT (Stetson 1987). We identified stars with intensities above 5 times the r.m.s. noise of each image using DAOFIND, then aperture photometry was performed on the selected stars with a circular aperture of 3 pixel radius (0.23 arcsec). A Point-spread function (PSF) was fitted using bright and isolated stars in each image. Then, the instrumental magnitude was derived for each identified star using the fitted PSF in each image. We subtracted the identified stars off the original image and we run DAOFIND again in the residual image to select fainter stars that were not identified in the original images. The magnitudes of these new stars were derived and included in the final photometry. In this second iteration of DAOPHOT we detected the following stars in each filter, 22 stars in F205W, 41 stars in F160W and 47 stars in F110W. However, we are only modelling stars detected in the 3 NICMOS filters. With this condition the second iteration add only 5 stars to the sample in the models. None of these 5 stars are in the group classified as WR, RSG or massive OB stars, and therefore it does not have impact in the analysis nor conclusions presented in the paper. Aperture corrections to a radius of 0.49 arcsec were applied to the instrumental magnitudes in order to use the photometric calibrations recorded in the image headers and provided by the NICMOS team². Finally, magnitudes in the Vega system for each star and each filter were then obtained.

The result of the stellar photometry is shown in the top panels of Fig. 2. We present here the colour-colour and CMD for the identified stars in NGC 604. The magnitude errors are a combination of the image photon noise and the uncertainties derived from the PSF fitting procedure and from aperture corrections; these are shown as a function of the magnitude for each filter in the lower panels of Fig. 2. The red diamonds in the top panels of Fig. 2 correspond to the RSG candidates derived from the UVI photometry from Hunter et al. (1996). We identified the RSG candidates in the NICMOS images using the coordinates of Hunter et al.'s star catalogue and the F555W image from their study. Only 6 candidates were within the field of view of NICMOS. With exception of one RSG candidate (number 2 in Table 2), for which we identified another star very close to it with magnitudes in all NICMOS filters and with no counter part in the UVI photometry, the rest of the stars are clearly identified as single stars in the NICMOS images. For the star 2 in Table 2 we added the IR fluxes of the two identified stars in order to perform the SED fitting with all the filters available (see section 3).

¹ <http://stdas.stsci.edu/multidrizzle>

² <http://www.stsci.edu/hst/nicmos/performance/photometry>

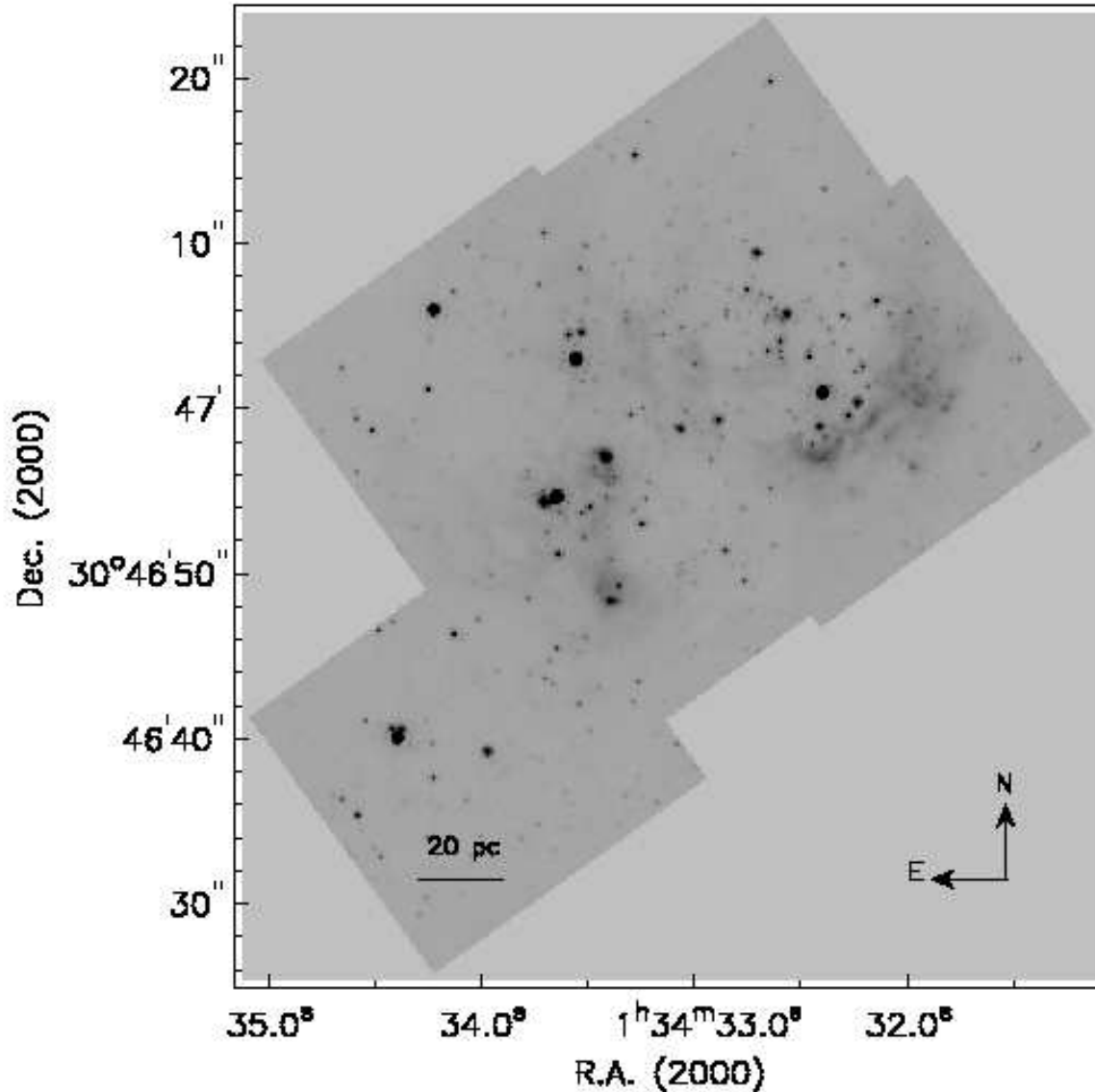


Figure 1. Final mosaic F205W image of NGC 604 obtained with NICMOS-NIC2 Camera. The total field of view of NICMOS observations is $50'' \times 60''$ with a pixel scale of 0.075 arcsec.

2.2 Confusion with foreground stars

The identification of RSGs in extragalactic clusters is a difficult task as they could be confused with foreground Galactic stars. As it has been explained in Massey (1998), a $40 M_{\odot}$ RSG in M33 would have an apparent magnitude in V-Band between +15.5 to +18, depending on its effective temperature. For dwarf late-type stars the absolute V magnitude is +6 (for a K0 dwarf star) and +12 (for a M5), taking ~ 600 pc as the estimated distance for these stars in the direction of M33, the apparent V magnitudes for these stars will be between +15 and +21 (Massey 1998). Therefore, it is possible to mistake a Galactic dwarf late-type star for a RSG in M33.

A method of separating foreground stars from RSGs based on IR two-colour diagrams have been proposed by

Elias & Frogel (1985): the RSG are 0.1-0.2 mag redder than late-type dwarfs in J-H at comparable H-K. In Fig. 3 we show the JHK colour-colour diagram for the stars with NICMOS photometry as well as for the RSG candidates. The magnitudes in the NICMOS filters have been converted into magnitudes in the JHK system following the transformation of Brandner et al. (2001). Since the magnitude conversion procedure already adds uncertainties in the magnitude we only convert those stars with magnitude errors lower than 0.2 mag. The blue line denotes the location of the foreground late-type dwarf stars with magnitudes obtained from Koornneef (1983). Clearly four of our RSG candidates stand between 0.2 to 0.6 magnitudes above the location defined by the foreground stars. The two stars that lie below the line defined by the foreground stars are S2 and S5. These stars,

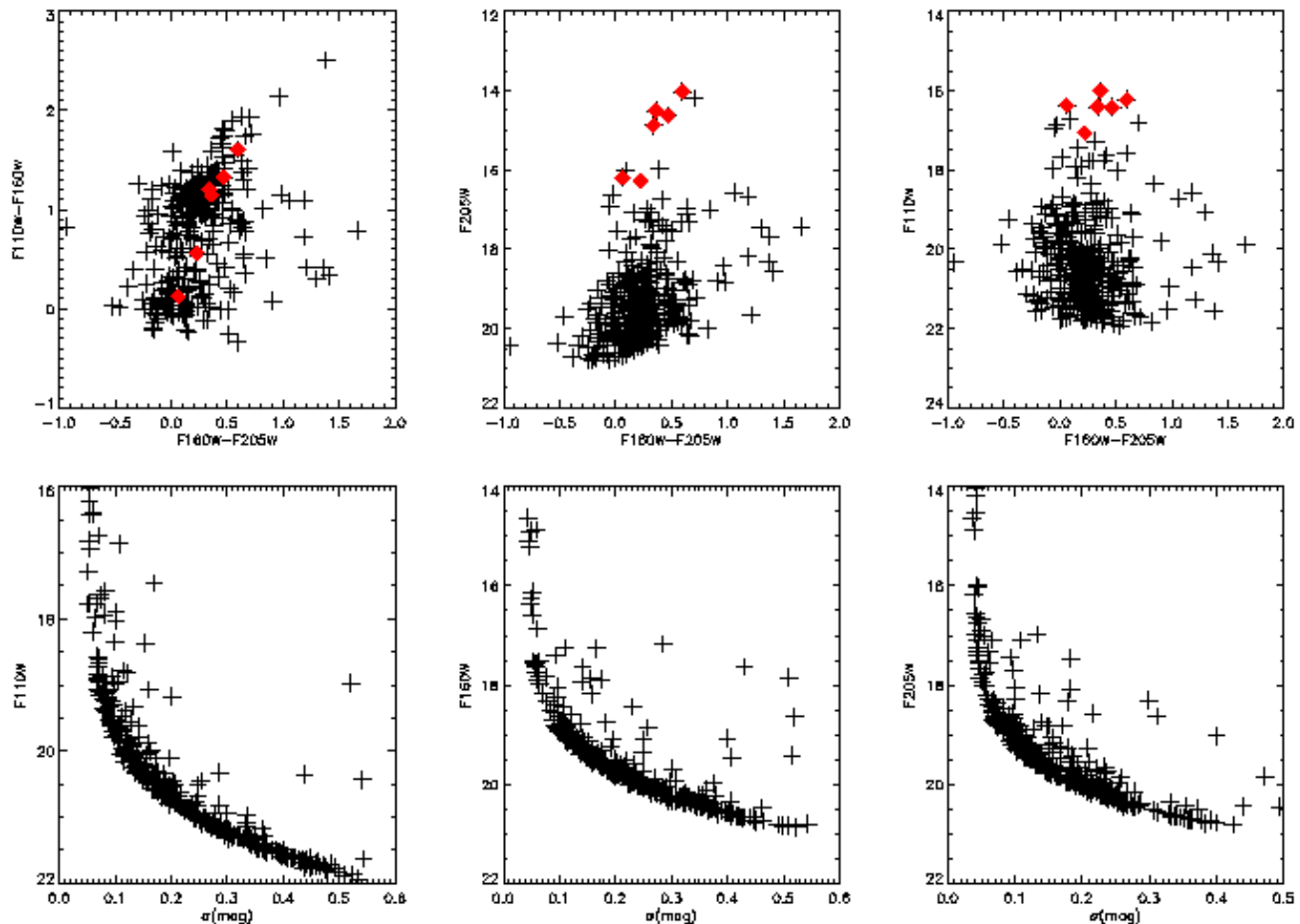


Figure 2. Top panel: Colour-colour diagram (left) and CMDs (centre and right) for NGC 604 in the NICMOS filters F110W, F160W and F205W. The red diamonds are the candidate RSG stars selected using the UVI stellar photometry from Hunter et al. (1996). Bottom panel: Observed magnitude as a function of the estimated errors for each filter: F110W (left), F160W (centre) and F205W (right). No extinction corrections have been applied to the magnitudes and all the magnitudes are in the Vega system.

as we will see later, have anomalous SED fitting (see section 4).

3 STELLAR EVOLUTION MODELS AND SED FITTING

Determining the physical parameters of stars from photometry requires a combination of stellar evolution models, model stellar atmospheres and a method to find the best fit between models and theory. In this section we outline the stellar and atmosphere models, their amalgamation and how we use the results to estimate parameters for the observed stars. To calculate the absolute magnitudes of the observed stars we take the distance of NGC 604 to be 840 kpc (Freedman et al. 1991).

We use stellar models from the Cambridge STARS code (Eldridge, Izzard & Tout 2008, and references therein) that have been correlated with stellar atmosphere models to produce synthetic spectra and broad-band photometric colours as described in Eldridge & Stanway (2009). Their key feature is that there is not only a set of detailed single star models, but also an extensive set of detailed binary star models

which are key to producing a realistic synthetic stellar population. We consider stellar models at the relevant metallicity for NGC 604 $Z=0.008$ (Vílchez et al. 1988; Esteban et al. 2009), where Z is the metallicity mass fraction (a metallicity of $Z=0.020$ is conventionally considered solar). It is well known that local metallicities within disk galaxies can vary by significant factors away from the mean host metallicity. We inspected the affect of varying metallicity by running the fits with models at metallicities of $Z = 0.004$ and 0.020 . We find that our results change only slightly and allowing the metallicity to vary would only increase the uncertainty of our results. We assume a hydrogen mass fraction of $X = 0.73$ and a helium mass fraction of $Y = 0.262$. We calculate observable magnitudes for these stellar interior models by using a model atmosphere that best represents the appearance of the interior model at each timestep. The atmosphere models are for OB stars, WR stars and other stellar types and they are described in Smith, Norris & Crowther (2002), Hamann, Gräfener & Liermann (2006) and Westera et al. (2002), respectively.

Given that stellar evolution is non-linear, and binary evolution is even more so, we do not interpolate between models with different initial parameters to determine the

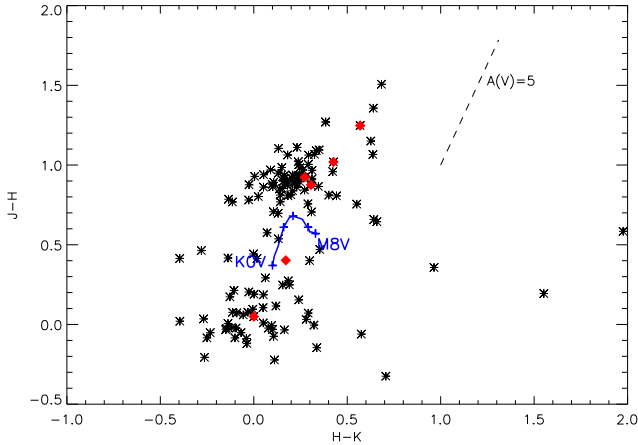


Figure 3. Colour-colour diagram in the JHK system for the stars identified in NICMOS images and magnitude errors less than 0.2 mag. Red diamonds correspond to the RSG candidates shown in Fig. 2. The blue line shows the location of foreground late-type dwarf stars. The transformation from the NICMOS filter to JHK system has been performed following the equations given in Brandner et al. (2001). The reddening vector corresponds to $A_V=5$ mag and the Cardelli, Clayton & Mathis (1989) extinction law.

nature of the observed stars. Instead, we compare the observed SEDs to the synthetic SEDs at every timestep of each stellar model and estimate a most likely mass, age and extinction for each observed star. This is done by calculating mean parameters from all the models that match the observed SED.

We first estimate the amount of extinction required for the synthetic SED to match the observed SED. We calculate the amount of extinction required in each band to achieve an exact match between the observed and model magnitudes. Using the Cardelli, Clayton & Mathis (1989) extinction curve we convert each magnitude to the equivalent extinction in A_V calculating the conversion factor α_i , such that $A_i = \alpha_i A_V$ for the i th filter. We then calculate the mean extinction from the six filters, as follows,

$$A_{v,n}(m, t) = \frac{1}{N} \sum_{i=1}^N \frac{(M_{\text{obs},n,i} - M_{\text{model},i}(m, t))}{\alpha_i}, \quad (1)$$

where the magnitudes predicted by a model are $M_{\text{model},i}(m, t)$ for a star with initial mass m and age t , the observed magnitude is $M_{\text{obs},n,i}$ for the n th star in the i th filter and N is the number of filters in which the source is detected. This mean extinction is then used to correct the synthetic SED magnitudes for dust.

This dust corrected model magnitudes,

$$M_{\text{model,cor},i,n}(m, t) = M_{\text{model},i}(m, t) + \alpha_i A_{v,n}(m, t), \quad (2)$$

are then used to calculate the probability, $p_n(m, t)$, of a match between the observed SED and theoretical SED can be evaluated as follows:

$$p_n(m, t) = \prod_{i=1}^6 \exp\left(-\frac{(M_{\text{model,cor},i,n}(m, t) - M_{\text{obs},n,i})^2}{2\sigma_{\text{total},i}^2}\right) \quad (3)$$

The errors are therefore assumed to be Gaussian. σ_{total} is

calculated as a combination in quadrature of the error in the photometry and an assumed error in the stellar models of 0.3 mag. This error is estimated from the magnitude difference between two stars of neighbouring masses in our grid of models. We must also take into consideration the resolution of our mass grid in the probability calculation. For example our $15M_{\odot}$ model has neighbouring model masses of 14 and $16M_{\odot}$. While the $80M_{\odot}$ model has neighbours in the mass grid of 70 and $100M_{\odot}$. Therefore we add a factor, $\Delta m(m)$, to the probability to give every mass an equal probability. For the the 15 and $80M_{\odot}$ examples this factor would be 1 and 15 respectively.

The last factor to consider in the likelihood of a match is how quickly stars evolve. Two stars might have the same apparent SED but one is evolving more rapidly than another. A star evolving slowly, such as main-sequence stars will be more probable matches to a SED than a short-lived WR stars. Therefore we use the probability and the timestep of each model SED as a weight to estimate values for the parameters of each observed star. For example, the mass (M_n), age (τ_n) and extinction ($A_{v,n}$) are obtained as follows:

$$M_n = \frac{\sum_m \sum_t m \Delta t(m, t) \Delta m(m) p_n(m, t)}{\sum_m \sum_t \Delta t(m, t) \Delta m(m) p_n(m, t)} \quad (4)$$

$$\tau_n = \frac{\sum_m \sum_t t \Delta t(m, t) \Delta m(m) p_n(m, t)}{\sum_m \sum_t \Delta t(m, t) \Delta m(m) p_n(m, t)} \quad (5)$$

$$A_{v,n} = \frac{\sum_m \sum_t A_{v,n}(m, t) \Delta t(m, t) \Delta m(m) p_n(m, t)}{\sum_m \sum_t \Delta t(m, t) \Delta m(m) p_n(m, t)} \quad (6)$$

and for each of these we are able to estimate an error from the variance, for example:

$$\sigma_{M,n}^2 = \frac{\sum_m \sum_t m^2 \Delta t(m, t) \Delta m(m) p_n(m, t)}{\sum_m \sum_t \Delta t(m, t) \Delta m(m) p_n(m, t)} - M_n^2 \quad (7)$$

Thus for each observed SED we obtain an estimate of age, initial mass, extinction, luminosity, surface temperature, the mass ratio ($q = M_2/M_1$) for the binary models and an error for each value. We note that we are only determining three independent parameters from each fit: luminosity, surface temperature and extinction. The age and mass are model dependent and linked to the surface temperature and luminosity. If we re-ran the analysis with different or updated models the luminosity, surface temperature and extinction would remain similar but the age and mass would change by a greater degree.

We perform our fitting process using two sets of models: single star models and binary models, then we compare the probability from the two fits to determine which is more likely. We find, except for the RSG1, 4 and 6, the binary models give a *better* match for all the stars we fit. This is likely to be due to the fact the binary models can cover more of the Hertzsprung-Russel diagram than the single stars therefore have a greater chance of achieving a close match to the SED. In most cases the likelihood difference between single and binary models is minimal up to only factors between 1 to 3. The only two fits for which binaries are significantly favoured are RSG3 and WR1. For these two stars they are 700 and 30 times more likely to be binaries respectively.

The SED fits for the RSGs and WR stars assume that

the stars are post-main sequence objects and therefore we only use post-main sequence models to prevent the fits being affected by main-sequence models skewing the fit. This is because in weighing by the timestep a WR star and a main-sequence OB star might have very similar SEDs but a star is more likely to be a main-sequence star due to its slow evolutionary timescale.

In Figure 4 we show examples of the location of possible SED matches on the Hertzsprung-Russel diagram. Then Figure 5 compares the theoretical SEDs from the same fits to the observed SED. For the red supergiant the surface temperature is tightly constrained but the luminosity is less well constrained. The more luminous models require more extinction to achieve the same SED and so tend towards higher surface temperatures. However, despite this large apparent degeneracy, a low luminosity around $10^5 L_\odot$ is preferred because of the consideration of the timestep. While there are many possible values of the luminosity, there is only one place where the star may be observed for an appreciable period of time. Therefore the fitting process gives greatest weight to this region and therefore gives the masses and ages listed in Table 2 below. In this Figure we also include a similar plot with the timestep weight removed from the SED fit. Without the timestep weight a better match is achieved by the more luminous and hence more massive RSG.

We note that in Figure 4 we predict more massive RSGs than other stellar evolution models such as Meynet & Maeder (2003). However the lifetimes of these massive RSGs are very short due to their high mass-loss rate and so they are unlikely to be observed. Furthermore the evolution of these massive RSGs is also uncertain and extra pulsation driven mass-loss may shorten their lifetimes further (Yoon & Cantiello 2010).

For the WR star the region on the surface temperature is less well constrained. This is not surprising as these stars are hot and with the filters used in the SED fitting we are only looking mainly at the Rayleigh-Jeans tail of the black-body spectrum so there is little constraint on the surface temperature. Therefore the SED fits of the WR and main-sequence stars are intrinsically less well constrained. Furthermore in Figure 5 the agreement between the observed and theoretical SEDs is slightly poorer, especially in the J and H filters. This is due to most of the WR flux being output at shorter wavelengths so the IR flux may be more greatly effected by IR emission from other nearby sources.

An important check to understand the accuracy of the SED fitting process is to feed theoretical models through the SED fitting code and compare the output to known inputs. The models we use to do this were calculated separately to have initial masses between the mass grid of our stellar models. We use single star models with initial masses of 65, 90 and $100M_\odot$. We also include a $150M_\odot$ model to understand how stars above our maximum model mass would appear. We calculate fits to the models at three evolutionary phases, the main-sequence, RSG phase and the WR phase. The results of these fits are shown in Table 1.

The fits on the RSG phase are most accurate as it is possible to achieve a better match for cooler stars. This is because the peak of black-body spectrum is observed rather than for hotter stars where only the Rayleigh-Jean tail of the black-body spectrum is covered. Thus both the main-

Table 1. Results of test of SED fits for stellar models not in our standard grid. The evolutionary phases are, MS main sequence, RSG - red supergiant and WR - Wolf-Rayet.

Model mass $/M_\odot$	Single star fit M_i/M_\odot	Binary fit M_i/M_\odot	Evolutionary Phase
65	85 ± 26	79 ± 25	MS
65	60 ± 5	55 ± 9	RSG
65	97 ± 21	83 ± 29	WR
90	63 ± 15	54 ± 17	MS
90	98 ± 18	103 ± 19	RSG
90	90 ± 20	85 ± 28	WR
110	89 ± 25	98 ± 24	MS
110	88 ± 14	89 ± 21	RSG
110	85 ± 25	80 ± 31	WR
150	87 ± 24	85 ± 25	MS
150	106 ± 10	104 ± 17	RSG
150	85 ± 25	80 ± 31	WR

sequence and WR fits are less accurate. However it is possible to explain the inaccuracy of the the 65 and $80M_\odot$ fits. The the $65M_\odot$ SED was taken from towards the end of evolution for the star while the $90M_\odot$ SED was taken from the near beginning of the track. Therefore there is some degeneracy in the fitting of main-sequence stars between mass and age. In addition the more massive stars, including the $150M_\odot$ do tend to have their masses underestimated due to this mass-age degeneracy. Only with more information from the UV of the stars could we achieve a more accurate fit. An important conclusion here is that while individual fits will be uncertain by using the properties of all of the stars some of these errors will cancel out to provide a reasonable estimate of the mass and age of NGC 604.

This test indicates that the information inferred on the RSGs can be trusted more than that on the hotter stars. Also that while each individual fit may not give the exact result, if we take the entire population of stars into consideration our combined uncertainty in the total age and mass of a region is significantly reduced.

Another problem with our fit is due to weighing by the timestep a star in a rapid phase of evolution may be misidentified as a lower mass, more slowly evolving, star. Therefore we removed the Δt from the fitting process. We found that the resulting values were similar to those when the timestep is included. The only exception was RSG1. In Table 2 we show that the mass of the RSG changes from $23 \pm 20 M_\odot$ to $67 \pm 36 M_\odot$ with a corresponding drop in age and increase in extinction. Such a massive RSG has a very short evolutionary timescale which is why it is not favoured when the timestep weight is included. It is not possible from SED fitting alone to determine which mass is the best solution even though the more massive, shorter lifetime, RSG fit is less probable. To determine its true identity a spectrum of the star is required. However we assume its has a similar age to the other RSGs in our analysis of the region and we note that its location (Fig. 9) is close to the centre of NGC 604 and suggests that the more massive solution is possible.

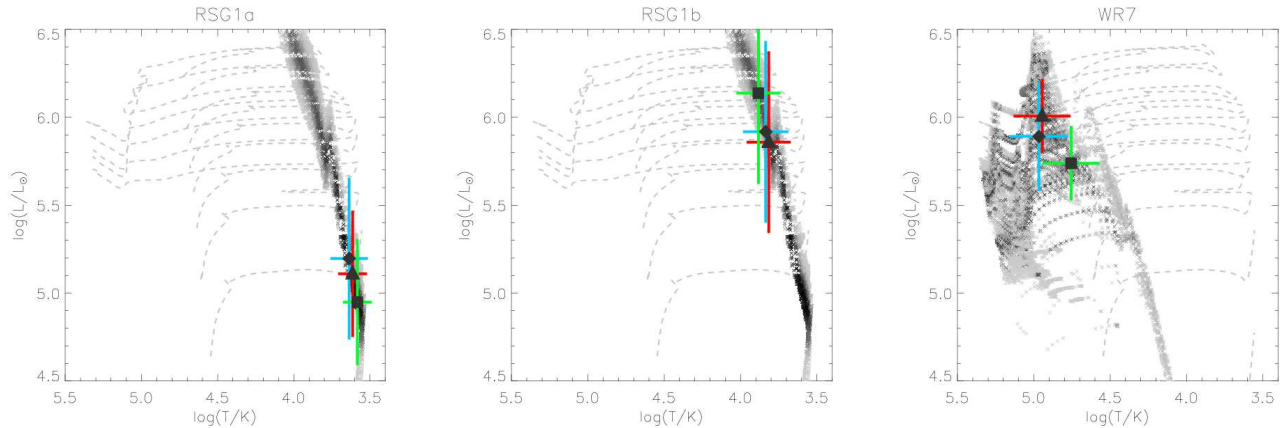


Figure 4. Examples of the region on the theoretical Hertzsprung-Russell diagram where models match the observed SEDs of RSG1 and WR7. We include two plots for RSG1 showing the two fits with and without timestep weighing, RSG1a and RSG1b respectively. The dashed grey lines indicate single star stellar models with masses of 10, 20, 30, 40, 50, 60, 70, 80, 100 and $120M_{\odot}$. The grey points indicate the regions where a SED match is made, the darker the point the better the agreement between the observed and model SED. The square with green error bars indicates the SED fit with the highest value of $m\Delta t(t)p_n(m, t)$ from both the single star and binary models. The triangle with red error bars indicates the mean T_{eff} and L estimated from the single models and the diamond with blue error bars indicates the mean T_{eff} and L estimated from binary models.

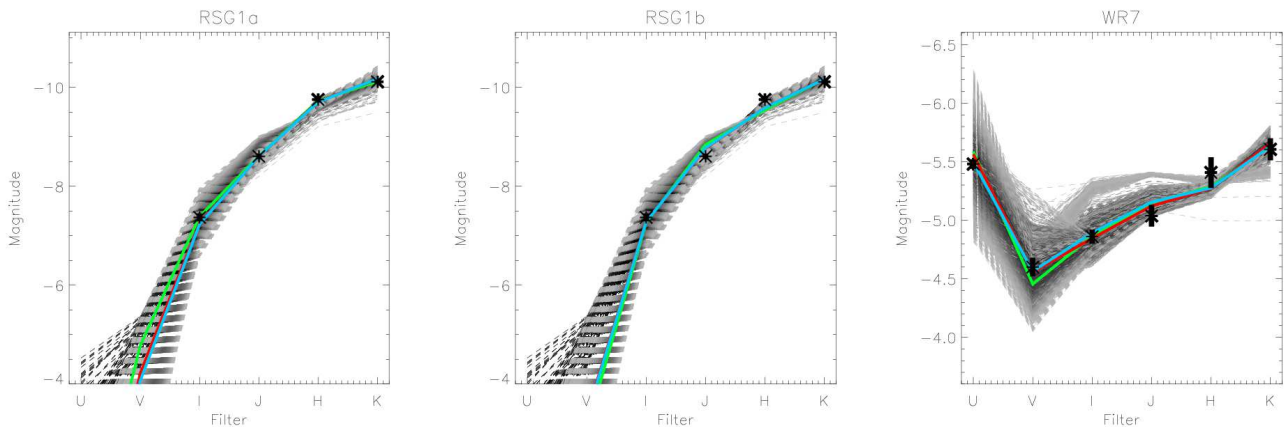


Figure 5. Comparison of the observed and theoretical SEDs for the two solutions of RSG1 and WR7. The dashed grey lines are theoretical matches to the observed SED, the darker the line the higher the probability of a match. These lines are the SEDs for the grey points in Figure 4. The green line is the theoretical SED with the highest value of $m\Delta t(t)p_n(m, t)$. The red line indicates the mean SED estimated from the single models and the blue line indicates the mean SED estimated from binary models. These three lines correspond to the colours points in Figure 4. The asterisks represent the observed SED, the vertical lines represent the uncertainty in the observed magnitudes.

4 RED SUPERGIANTS IN NGC 604

From Fig. 2 we find that there are at least four RSGs within NGC 604. Determining their ages is vital to understanding the star-formation history of this region. The results of the SED fitting are shown in Table 2. We see that, ignoring the unlikely younger fit for RSG1, the RSGs all have ages in the range of 10 to 15 Myrs with masses between 14 to $23M_{\odot}$. These are the typical ages and masses expected for RSGs (Levesque et al. 2005). One important result is that RSGs 1, 4 and 6 have a large extinction excess above that one predicted from the extinction map derived in Relaño & Kennicutt (2009). In Fig. 7, we plot the expected extinctions of the stars versus the values derived from SED fitting. Each of these stars is luminous with a bolometric

magnitude in the F205W filter (similar to K-band) of ≈ -10 . Such extinction excess is found to be typical for RSGs with similar luminosities (Massey et al. 2005). The excess is explained as intrinsic extinction from dust produced in the RSG atmosphere and stellar wind. A final detail to note is that RSG3 is significantly better fit by a binary model than a single star.

The second solution for RSG1 with a younger age and higher mass also has a greater extinction excess. Again this is not unusual when compared to the excesses found in Galactic RSGs (Massey et al. 2005). However, if this solution is true, then this star could be the most luminous RSG in the local group, as recent observations indicate that the maximum observed luminosity for typical RSGs is around $\log(L/L_{\odot}) \approx 5.3$ (Massey et al. 2005). Although due to its

Table 2. Results of the SED fitting of the most massive RSG and WR stars in NGC 604. We also show the results for the most luminous stars in the Hunter’s catalogue. Note that RSG2 and RSG5 may also be foreground stars and we list the two possible solutions to the SED fit for RSG1.

ID	M/M_{\odot}	Age/Myr	A_V	ΔA_v	$\log(L/L_{\odot})$	$\log(T/K)$	$q = M_2/M_1$	Spectral Type
RSG1 _a	23 ± 20	11.5 ± 3.2	2.7 ± 1.9	2.5	5.1 ± 0.4	3.61 ± 0.09	-	
RSG1 _b	67 ± 36	5.7 ± 5.1	6.4 ± 2.4	6.2	5.9 ± 0.5	3.8 ± 0.2	0.5 ± 0.3	
RSG3	14 ± 2	15.0 ± 2.0	1.1 ± 0.4	0.3	4.8 ± 0.1	3.59 ± 0.02	0.8 ± 0.1	
RSG4	20 ± 3	10.2 ± 1.0	3.8 ± 0.4	3.0	5.2 ± 0.1	3.58 ± 0.02	-	
RSG6	16 ± 5	12.9 ± 1.8	2.7 ± 0.6	1.5	5.0 ± 0.1	3.59 ± 0.04	-	
S2?	101 ± 24	3.8 ± 4.5	3.6 ± 0.8	2.7	6.3 ± 0.4	4.3 ± 0.1	0.6 ± 0.3	
S5?	93 ± 19	3.2 ± 0.7	3.5 ± 0.2	3.3	6.3 ± 0.2	4.2 ± 0.1	0.7 ± 0.3	
WR1	100 ± 21	3.3 ± 0.7	0.8 ± 0.4	0.5	6.0 ± 0.2	5.0 ± 0.2	0.8 ± 0.2	WCE
WR2A	95 ± 25	3.4 ± 0.7	1.1 ± 0.3	0.8	5.9 ± 0.3	4.8 ± 0.3	0.8 ± 0.2	WN
WR2B	78 ± 26	3.6 ± 0.7	0.2 ± 0.2	-0.1	6.0 ± 0.2	4.6 ± 0.3	0.7 ± 0.3	WN
WR3	94 ± 26	3.3 ± 0.6	1.1 ± 0.3	0.9	6.0 ± 0.2	4.8 ± 0.3	0.8 ± 0.2	WN
WR5	38 ± 20	6.3 ± 2.0	0.4 ± 0.4	0.2	5.4 ± 0.3	4.8 ± 0.3	0.4 ± 0.3	WC6
WR6	80 ± 20	3.4 ± 0.7	1.6 ± 0.3	1.3	6.1 ± 0.2	4.4 ± 0.1	0.5 ± 0.3	WNL
WR7	79 ± 32	3.9 ± 1.2	1.3 ± 0.4	0.3	5.9 ± 0.3	5.0 ± 0.2	0.4 ± 0.3	WC4
WR8	57 ± 32	4.9 ± 1.6	0.2 ± 0.3	-0.2	5.7 ± 0.3	4.7 ± 0.3	0.5 ± 0.3	WN
WR10	67 ± 34	4.5 ± 1.5	0.2 ± 0.3	-0.2	5.8 ± 0.3	4.8 ± 0.3	0.5 ± 0.3	WN6
VI	92 ± 26	3.4 ± 0.7	0.5 ± 0.3	0.2	6.0 ± 0.2	4.8 ± 0.3	0.8 ± 0.2	Of/WNL
H38	91 ± 26	2.6 ± 1.1	0.5 ± 0.3	0.3	6.1 ± 0.2	4.6 ± 0.2	0.6 ± 0.3	
H40	80 ± 28	2.1 ± 1.6	0.2 ± 0.2	0.0	6.0 ± 0.2	4.6 ± 0.2	0.5 ± 0.3	
H367	102 ± 21	2.8 ± 0.6	1.0 ± 0.2	0.8	6.3 ± 0.2	4.4 ± 0.2	0.6 ± 0.3	
H368	98 ± 19	2.8 ± 0.6	1.0 ± 0.3	0.7	6.3 ± 0.2	4.4 ± 0.2	0.6 ± 0.3	
H369	89 ± 26	2.8 ± 1.0	0.5 ± 0.3	0.3	6.1 ± 0.2	4.6 ± 0.2	0.5 ± 0.3	
H371	91 ± 28	2.2 ± 1.2	0.3 ± 0.3	0.1	6.1 ± 0.2	4.6 ± 0.2	0.5 ± 0.3	
H375	81 ± 27	2.0 ± 1.5	0.2 ± 0.2	0.0	6.0 ± 0.2	4.6 ± 0.2	0.5 ± 0.3	
H376	83 ± 28	2.1 ± 1.6	0.4 ± 0.3	0.1	6.0 ± 0.2	4.6 ± 0.2	0.5 ± 0.3	
H377	85 ± 29	2.6 ± 1.9	0.5 ± 0.4	0.3	6.0 ± 0.3	4.7 ± 0.3	0.5 ± 0.3	

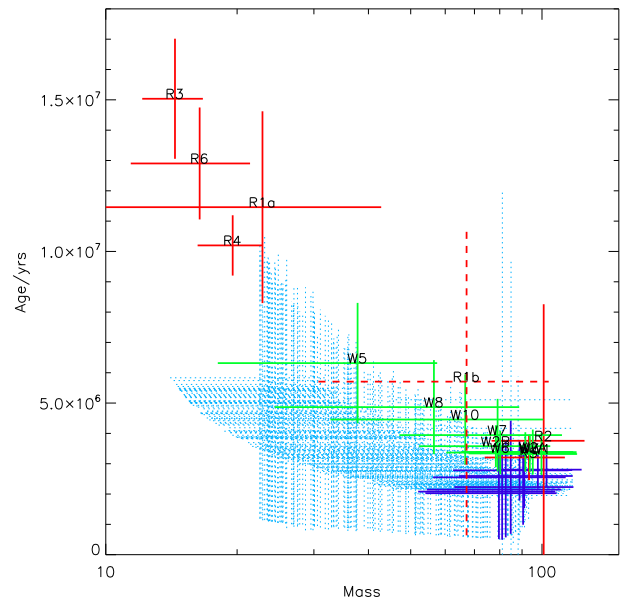
higher surface temperature it would probably be classified as a yellow supergiant (YSG). Its mass and age would be consistent with the hotter stellar population described below. However, only a spectrum of the object will truly confirm its nature, as it is the case for RSG4, the star spectroscopically confirmed as a RSG in Terlevich et al. (1996).

The two impostors RSGs S2 and S5 are most likely to be foreground stars as discussed above. The SED fit gives masses for the stars similar to the WR and OB stars in NGC 604. Their large extinctions are similar to the magnitude of the RSGs so they may be transition objects either becoming WR stars or leaving the main-sequence to become the RSGs. Only a spectrum for these objects can reveal their true nature.

In summary, the mean age of the RSGs 1, 3, 4 and 6 is 12.4 ± 2.1 Myrs and the mean initial mass is $18 \pm 4M_{\odot}$. The other two suspected RSGs are not RSGs but probably foreground stars.

5 WOLF-RAYET STARS IN NGC 604

In NGC 604 there are a number of spectroscopically confirmed WR stars (Drissen et al. 2008). From the available photometry we are able to perform a SED fit for 10 of these objects and the results are shown in Table 2. The derived ages and masses are remarkably consistent, with only WRs 5 and 8 being significantly different from the mean mass and

**Figure 6.** The age and mass values derived from the SED fitting for the RSGs (red), WR stars (green) and main-sequence stars (blue). The lighter blue points are based on UVI SED fitting alone. The names of the RSGs and WR stars are given.

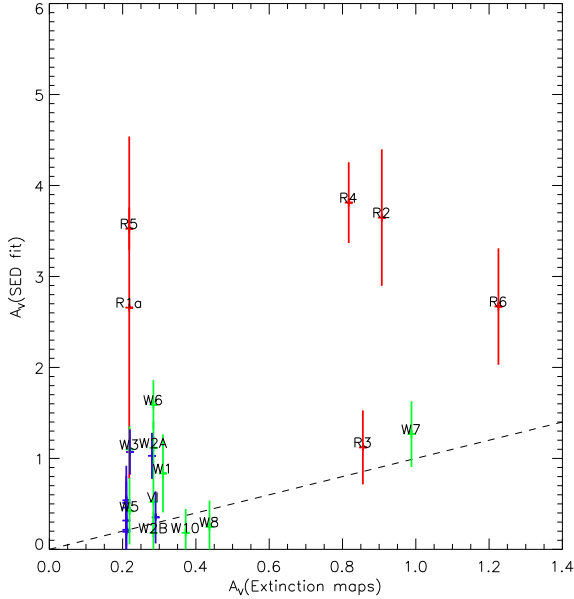


Figure 7. Extinction comparison between the values obtained from the Balmer extinction map of Relaño & Kennicutt (2009) and those derived here from the SED fitting. The observations are colour coded so that the RSGs are red, WR stars are green and main-sequence stars are blue. The names of the RSGs and WR stars are given.

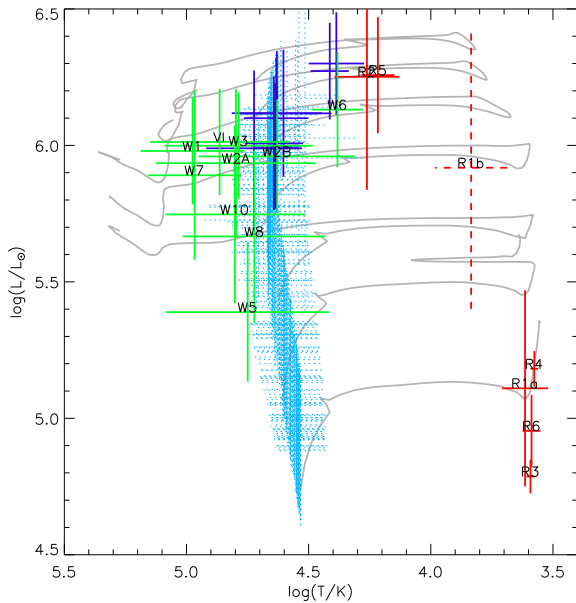


Figure 8. The theoretical Hertzsprung-Russell diagram for NGC 604. The single-star models in grey have masses of 20, 30, 40, 60, 80, 100, 120 M_{\odot} . Colour code is: red for RSGs, green for WR stars and blue for main-sequence stars. The lighter blue points are based on UVI SED fitting alone, names for the RSGs and WR stars are given. The R1b star is the second more luminous fit for RSG1. It also has a slightly higher surface temperature. Its location on the Hertzsprung gap means if this is a solution the stars is in a rapid phase of evolution.

age of all the WR stars. For each of the stars there is also a best fit with massive companions with a mass ratio of 0.5 to 0.8.

The WR stars have little excess extinction. We plot the expected extinction of the stars versus the values obtained from SED fitting in Fig. 7. We see that the WR stars correspond with the extinction derived in Relaño & Kennicutt (2009). This is to be expected as any dust around the star created during its brief RSG phase will be quickly swept away by the fast and dense WR winds (e.g. Eldridge et al. 2006). The case with the highest extinction, WR6, is identified as a WNL star. These stars are thought to have still some of their remaining hydrogen envelope and therefore will not have completely removed all the dust from their immediate vicinity. This is consistent with the evolutionary scenario of a star being a RSG before becoming a WNL star.

The consistent ages and masses of the fits to the WR stars suggest that they were all formed in a single and recent burst of star-formation with a mean age of 4.0 ± 1.0 Myrs. This is significantly different to the RSG ages shown above but it is also similar to the age inferred for RSG2 and RSG5 and the alternative fit for RSG1. The mean initial mass for the WR stars is $76 \pm 10 M_{\odot}$.

6 MAIN-SEQUENCE STARS IN NGC 604

In the photometric catalogue of Hunter et al. (1996) there are 1040 stars with UVI photometry. We have performed a similar process of SED fitting for the entire catalogue using these three filters. Because most of these stars are main-sequence objects the inclusion of JHK photometry does not increase the accuracy of our fit. However, for a sample of the most luminous stars in the catalogue we have also performed a 6 filter fit and listed the results in Table 2. The estimated parameters agree within the fit errors. From the fit of the entire catalogue, we find 34 O stars with masses above $70 M_{\odot}$, with the most massive star $\approx 100 M_{\odot}$. For these 34 stars we find a typical age of 2.4 ± 0.3 Myrs. Below $70 M_{\odot}$ the error in the age of the SED fit increases significantly, as shown in Fig. 6, because of the degeneracy between mass and age for O stars. For example above $60 M_{\odot}$ we find 53 stars with a mean age of 2.8 ± 1.1 Myrs.

In most cases of the OB stars the derived extinction is similar to that seen across the NGC 604 region as derived by Relaño & Kennicutt (2009). This is as expected with the OB star winds being fast and sweeping out the region around each star.

In both mass range mentioned above the ages are slightly younger than the ages derived for the WR stars but still overlapping within the errors. This is to be expected because both the OB and WR stars come from the same initial mass range but are respectively earlier/later in their relative lifetimes. We created synthetic cluster models of NGC 604 formed in a bursts lasting between 1 to 2 Myrs. We find that in these models the true age of the cluster is between the ages of the OB and WR star populations with the same initial masses. In addition the duration of the burst is similar to the spread of the two ages of the two populations.

It is worth noting that the apparent spread also has another possible explanation the stars might have different rotation rates with those rotating more rapidly having longer

main-sequence lifetimes. If this is the case then the duration of the star-formation burst would be decreased.

7 STELLAR POPULATION OF NGC 604

From the analysis shown above we see that NGC 604 is a collection of main-sequence stars, RSGs, possible BSGs and WR stars. We find two distinct populations: an older one with an age of 12.4 ± 2.1 Myrs represented by the RSGs, and a younger one which is a combination of O stars, possible massive RSG/BSGs and WR stars with a mean age of 2.4 ± 0.3 Myrs for the O stars and 4.0 ± 1.0 Myrs for the WR stars. We take the age of this younger population to be 3.2 ± 1.0 Myrs by combining these last two measurements assuming that the true age of the burst is intermediate between the relatively *young* O and *old* WR stars. Importantly the WR stars indicate the upper age for the star formation burst to be around 5 Myrs. This can be visually checked in Figure 6 with the ages clustered closely around 2 to 4 Myrs.

We plot our results for the estimated luminosities and surface temperatures onto a Hertzsprung-Russell (HR) diagram in Fig. 8. We see that many of the WR stars cluster around the track for the $80 M_{\odot}$, along with many of the most massive stars and S2 and S5. While RSG 1, 3, 4 and 6 are closer to the $20 M_{\odot}$ track. This again demonstrates that the RSGs in NGC 604 are a separate population from the more massive stars.

For the young and old populations it is possible to place limits on the total stellar mass formed in each population. Using the mean mass and its uncertainty to describe the mass range of the stars in each population, we can estimate the total mass of the stars assuming a Salpeter IMF (with $\alpha = -2.35$) from 0.5 to $120 M_{\odot}$ and a slope with $\alpha = -1.3$ between 0.1 and $0.5 M_{\odot}$ (Kroupa 2002). This only gives us the mass of primary stars, therefore we multiply the resultant mass by 1.5 to account for each star having a binary companion. Doing this we assume a flat distribution of the mass ratio between the two stars with $0 < M_1/M_2 \leq 1$. For the older population with 4 RSGs assuming they represent all stars between 14 and $22 M_{\odot}$ we find a total mass of $1700 \pm 900 M_{\odot}$. For the younger population with masses above $70 M_{\odot}$, we estimate a mass of $(3.8 \pm 0.6) \times 10^5 M_{\odot}$. We note that if we use all stars with masses above $60 M_{\odot}$ we obtain an identical mass estimate.

The stellar population of NGC 604 can also be investigated by using various spectral features in a integrated spectrum for all stars in the region. González-Delgado & Pérez (2000) obtained UV and optical spectra of the NGC 604 region and studied in detail the nebular emission of the region. Using their spectrum we have calculated the equivalent widths for the stellar population diagnostic lines of CIV at 1500 \AA , HeII at 1640 \AA and the Blue WR bump around 4686 \AA and compared them to those predicted by our synthetic spectra for the stellar populations. The calculation of the equivalent widths and the construction of the synthetic spectra are described in detail in Eldridge & Stanway (2009).

We plot the comparisons in Fig. 10. We see that the features that are dependent on the WR stars -the HeII line and Blue WR bump- are in agreement with the observed values are ages around 3 Myrs. The CIV line which is dom-

inated by emission from the main-sequence OB stars has agreement at much earlier ages of 1.5 Myrs. Therefore we can assume that there is some agreement between models and the observed spectra but there is no exact match. We suggest this is because the two spectra do not fully cover the whole area of NGC 604 and therefore we cannot be sure that the entire resolved population of stars is contributing to the spectrum observed. Also the model spectra are for an instantaneous burst where NGC 604 has an extended period of star-formation. However, the general agreement provides confidence in the synthetic binary population and spectral models.

8 H α AND LEAKAGE OF IONIZING PHOTONS

Using the masses for the stellar population given above and the predicted H α per M_{\odot} at different ages listed in Table 3 it is possible to estimate the H α flux these two populations will produce. We calculate the nebula emission from CLOUDY (Ferland et al. 1998) as described in Eldridge & Stanway (2009). The ionizing spectrum given to CLOUDY as input is obtained using the fitted stellar populations in this paper (Table 2) and the corresponding stellar interior and atmosphere models. The predicted flux varies most with the assumed age for the populations. For the old population we find $\log(F(\text{H}\alpha)/\text{erg s}^{-1}) \leq 36.75$, while for the younger population of 3.2 ± 1.0 Myrs we find $\log(F(\text{H}\alpha)/\text{erg s}^{-1}) = 39.92^{+0.11}_{-0.20}$. Therefore, it is the younger population the one which dominates the H α emission from NGC 604.

The H α flux from NGC 604 has been studied in detail by Relaño & Kennicutt (2009). They obtained an extinction-corrected H α of $\log(F(\text{H}\alpha)/\text{erg s}^{-1}) = 39.63 \pm 0.07$. Our model prediction agrees within the errors with this value, but in general overestimates the H α flux and we investigate this further.

Relaño & Kennicutt (2009), using the single-star *Starburst99* code (Leitherer et al. 1999) inferred the mass of stars in NGC 604 to be $5 \times 10^5 M_{\odot}$ assuming a Salpeter IMF between 0.1 and $120 M_{\odot}$. This value was derived using single star models and an age of 4 Myrs. Using the observed flux, our single star models and an age of 4 Myrs we also find a similar mass of $4.7 \times 10^5 M_{\odot}$. However, the uncertainty in the mass is greater for single star models because for them the H α flux varies more with age than for binary star models (see Table 3). The weaker variation of H α flux for binaries compared to that from single star models is due to rejuvenation of secondary stars and mergers from binary evolution.

The binary population models produce more H α flux per stellar mass over a longer period of time. As most of the stars in Table 2 are better fit with the binary population models we favour the H α flux prediction from these models. The difference in the predicted and observed H α flux gives us an estimate of the leakage fraction of ionizing photons. For NGC 604 we derive a leakage fraction of 49^{+16}_{-19} per cent of the total ionizing flux in the region.

This value of leakage is dependent on uncertainties within the stellar models. Alternative explanations for the mismatch of observed and predicted H α flux are therefore that either we are overestimating the number of massive

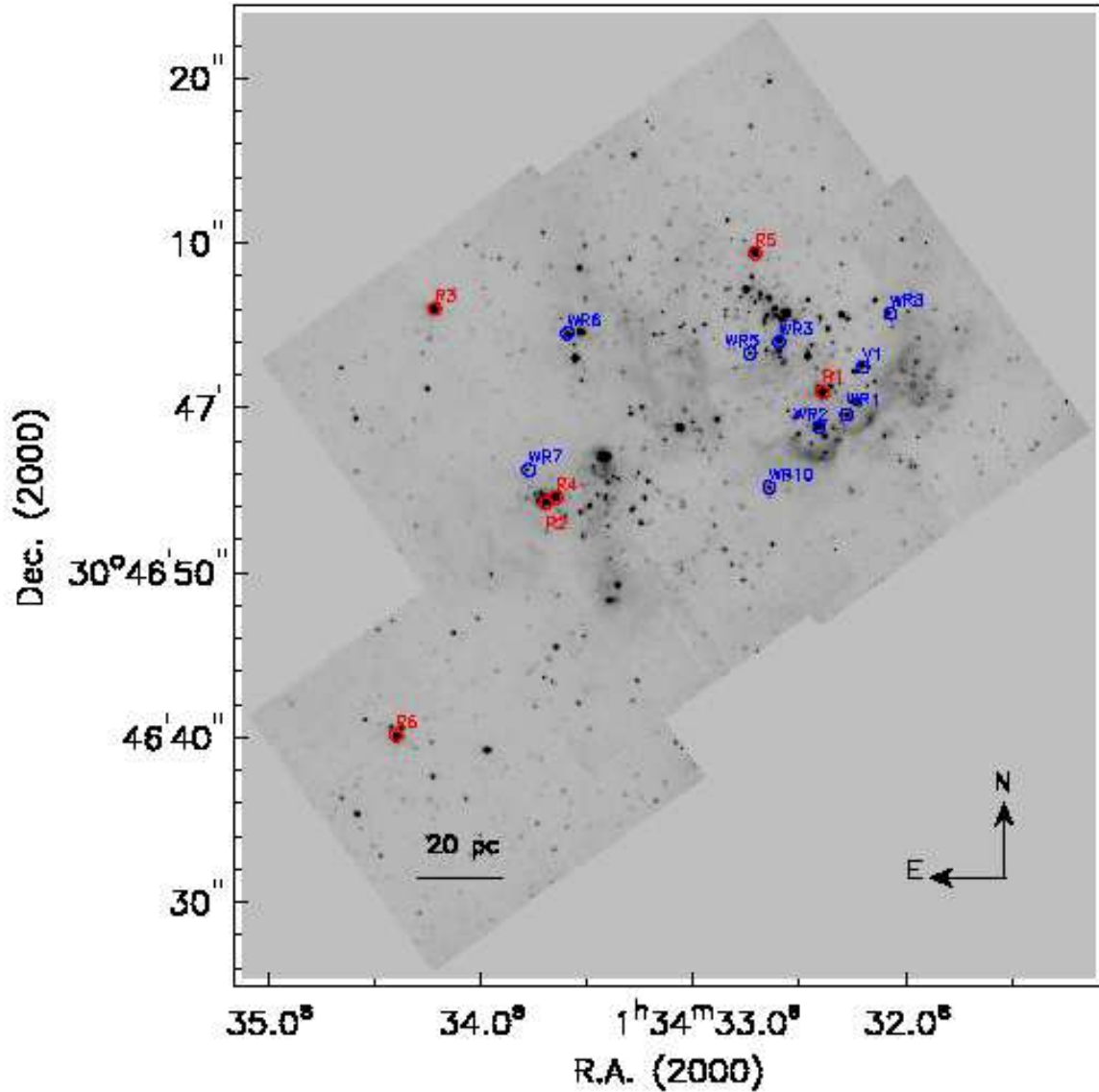


Figure 9. Final mosaic F110W image of NGC 604 with the WR stellar population (blue circles) from Hunter et al. (1996) and the RSG stars (red circles) identified in NICMOS data.

stars or the age of the region must be greater than 5Myrs. Both these possibilities reduces the $H\alpha$ flux from the stellar population. However, the large number of young main-sequence stars and massive WR stars indicates such an old age is unlikely. Therefore we can be confident in our results.

9 DISCUSSION & CONCLUSIONS

We have found further evidence that there is a population of RSGs within NGC 604. This older population inferred from the RSGs 12.4 ± 2.1 Myrs. The age of the more numerous young stars is 3.2 ± 1.0 Myrs, which is in agreement with previous studies (Maíz-Apellániz et al. 2004; González-Delgado & Pérez 2000).

There is some uncertainty in the nature of RSG1 as it

may be a very massive RSG or YSG in a short-lived phase of evolution. To accurately determine its mass a spectrum of this object is required. However its deep position in NGC 604 surrounded by many O and WR stars indicates that it may well be a very massive RSG.

The RSGs have larger extinctions than the other stars in NGC 604. This is in agreement with them producing large amounts of dust to obtain greater intrinsic extinction (Massey et al. 2005). The one WNL WR star also has a higher extinction than expected from the study of Relaño & Kennicutt (2009). This is in agreement with the evolutionary scenario that RSGs lose their hydrogen envelopes and become WR stars. The two stars labeled in Table 2 as S2? and S5? may be RSGs in the very late phases of losing their hydrogen envelopes due to their very high

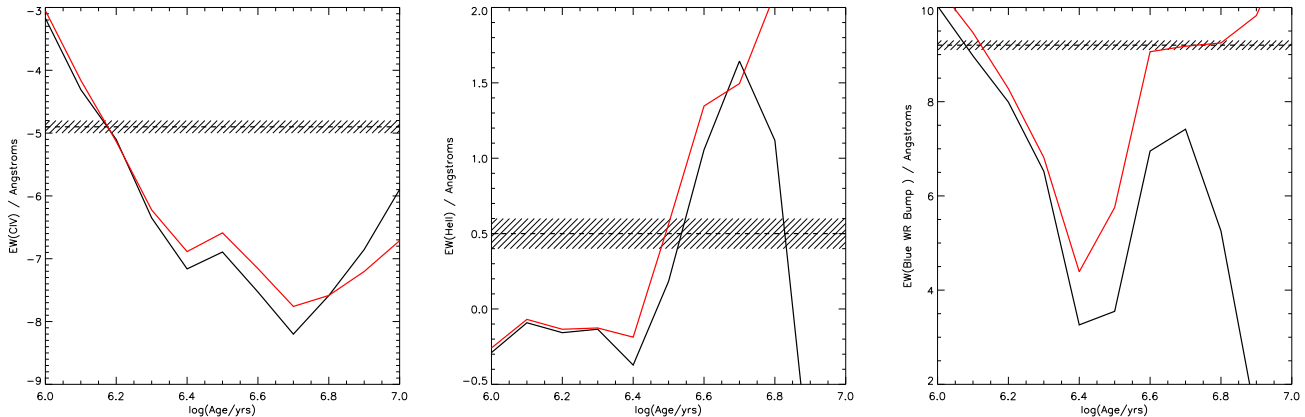


Figure 10. The equivalent widths of different stellar population diagnostic lines of NGC 604, the dashed lines with errors represented by the hashed region, compared to single-star (black) and binary (red) population models. Left: the CIV line at 1550 Å from O-stars, centre: the HeII line at 1640 Å from WR stars and right: the Blue WR bump around 4686 Å.

Table 3. Predicted $H\alpha$ flux per M_{\odot} of stars for both single star and binary populations.

$\log(\text{Age}/\text{yrs})$	$\log(F(H\alpha)_{\text{Single}})$ / $\text{erg s}^{-1}M_{\odot}^{-1}$	$\log(F(H\alpha)_{\text{Binaries}})$ / $\text{erg s}^{-1}M_{\odot}^{-1}$
6.0	34.34	34.41
6.1	34.35	34.43
6.2	34.35	34.44
6.3	34.35	34.43
6.4	34.25	34.39
6.5	34.16	34.34
6.6	33.96	34.20
6.7	33.67	34.02
6.8	33.27	33.83
6.9	32.75	33.54
7.0	32.27	33.34

inferred extinction. However they are more likely to be foreground stars.

We also find that the WR spectral features HeII and the Blue Bump and the O-star CIV P-Cygni profile of the composite spectrum of the region agree in general with the results from the resolved stellar population. The OB main-sequence stars appear to be younger than the WR stars. However, a direct comparison is difficult as the UV and optical spectra of the region do not cover the entire region and the duration of the star-formation burst is similar to the age of the cluster and therefore difficult to model.

By using the estimated age of the stellar population we are able to predict the $H\alpha$ flux from the massive stars and compare this to the flux observed for NGC 604. We find the two agree in magnitude but that 49_{-19}^{+16} percent of the ionizing flux may be escaping from the region. The greatest uncertainty in calculating the $H\alpha$ flux, and therefore the amount of leakage, is the age of the stellar population. Thus, we are unable to completely rule out that there are no absolute leakage of ionizing photons. However, since leakage has been studied to be a common property of luminous HII regions (e.g. Oey & Kennicutt 1997; Zurita et al. 2002; Relaño & Peimbert 2002), it is more likely that leakage is oc-

curing. Future study of the main-sequence population using HST/ACS data will enable tighter constraints to be placed upon the predicted ionizing flux escaping from NGC 604 (Laporte et al., in prep).

The evidence supporting the existence of RSGs in NGC 604 and their relation to the most recently formed stars is important because recent and future cutting-edge telescopes operate at these longer wavelengths (e.g. Spitzer, Herschel, JWST and the E-ELT). Soon all premier observatories will operate predominantly at IR wavelengths and therefore modelling and observation efforts must act now to address this observational shift. There are known problems with modelling near-IR emission (Maraston et al. 2006; Lanon 2008): typically it is found that for some star clusters ages derived from near-IR observations do not agree with those estimated from optical ones. The RSGs within NGC 604 are a key element required to study distance HII regions in the IR. The relative contributions of older RSGs and younger stars must be evaluated. Key to breaking any degeneracy will be the use of spectra and spectral lines such as the IR lines of RSGs and Wolf-Rayet stars (e.g. Crowther 2007; Davies et al. 2010). This implies that the study of distant HII regions at IR wavelengths will be challenging unless the contribution of such contaminants can be fully understood.

10 ACKNOWLEDGEMENTS

We would like to thank the referee Ben Davies for his constructive comments that have led to a much improved paper. We would like to thank Rosa González-Delgado for kindly provides us with the UV and optical spectra of NGC 604 shown here. Some of the data presented in this paper were obtained from the Multimission Archive at the Space Telescope Science Institute (MAST). STScI is operated by the Association of Universities for Research in Astronomy, Inc., under NASA contract NAS5-26555. Support for MAST for non-HST data is provided by the NASA Office of Space Science via grant NAG5-7584 and by other grants and contracts. Multidrizze is a product of the Space Telescope Science Institute, which is operated by AURA for NASA. This

research was supported by a Marie Curie Intra European Fellowship within the 7th European Community Framework Programme.

REFERENCES

- Barbá, R. H., Maíz-Apellániz, J. M., Pérez, E., Rubio, M., Bolatto, A., Fariña, C., Bosch, G., Walborn, N. R. 2009, *Ap&SS*, 324, 309
- Brandner, W., Grebel, E. K., Barbá, R. H., Walborn, N. R., Moneti, A. 2001, *AJ*, 122, 858
- Cardelli, J. A., Clayton, G., C., Mathis, J. 1989, *ApJ*, 345, 245
- Crowther P.A., 2007, *ARA&A*, 45, 177C
- Davies B., Kudritzki R.-P., Figer D.F., 2010, *MNRAS*, tmp, 946D
- Drissen L., Crowther P.A., Úbeda L., Martin P. 2008, *MNRAS*, 389, 1033
- Drissen, L, Moffat, A.F., & Shara, M. 1993, *AJ*, 105, 1400
- Eldridge J.J., Genet F., Daigne F., Mochkovitch R. 2006, *MNRAS*, 367, 186
- Eldridge J.J., Izzard R.G., Tout C.A. 2008, *MNRAS*, 384, 1109
- Eldridge J.J., Stanway E.R. 2009, *MNRAS*, 400, 1019
- Elias, J. H., Frogel, J. A. 1985, *ApJ*, 289, 141
- Esteban, C., Bresolin, F., Peimbert, M., García-Rojas, J., Peimbert, A., Mesa-Delgado A. 2009, *ApJ*, 700, 654
- Ferland G.J., Korista K.T., Verner D.A., Ferguson J.W., Kingdon J.B., Verner E.M., 1998, *PASP*, 110, 761
- Freedman W.L., Wilson C.D., Madore B.F., 1991, *ApJ*, 372, 455F
- González-Delgado R.M., Pérez E. 2000, *MNRAS*, 317, 6
- Hamann W.-R., Gräfener G., Liermann A. 2006, *A&A*, 457, 1015
- Hunter, D., Baum, W., O'Neil, E., Lynds, R. 1996, *ApJ*, 456, 174
- Koornneef, J. 1983, *A&A*, 128, 84
- Kroupa, P., 2002, *Science*, 295,82
- Lanon A., Gallagher J.S. III, Mouhcine M., Smith L.J., Ladjal D., de Grijs R., 2008, *A&A*, 486, 165L
- Levesque E.M., Massey P., Olsen K.A.G., Plez B., Josselin E., Maeder A., Meynet G. 2005, *ApJ*, 628, 973
- Leitherer C., et al. 1999, *ApJS*, 123, 3
- Maraston C., Daddi E., Renzini A., Cimatti A., Dickinson M., Papovich C., Pasquali A., Pirzkal N., 2006, *ApJ*, 652, 85M
- Massey P., Plez B., Levesque E.M., Olsen K.A.G., Clayton G.C., Josselin E. 2005, *ApJ*, 634, 1286
- Massey P., Silva D.R., Levesque E.M., Plez B., Olsen K.A.G., Clayton G.C., Meynet G., Maeder A. 2009, *ApJ*, 703, 420
- Massey P. 1998, *ApJ*, 501, 153
- Maíz-Apellániz, J. M., Pérez, E., & Mas-Hesse, J. M. 2004, *ApJ*, 128, 1196
- Meynet G., Maeder A., 2003, *A&A*, 404, 975M
- Oey, S. & Kennicutt R. C. 1997, *MNRAS*, 291, 827
- Relaño M., Kennicutt R.C. 2009, *ApJ*, 699, 1125
- Relaño M., Peimbert, M. 2002, *ApJ*, 564, 704
- Smith L.J., Norris R.P.F., Crowther P.A. 2002, *MNRAS*, 337, 1309S
- Stetson, P. B. 1987, *PASP*, 99, 191
- Terlevich E., Díaz A. I., Terlevich R., González-Delgado R. M., Pérez E., García Vargás M. L. 1996, *MNRAS*, 279, 1219
- Vílchez, J. M., Pagel, B., Díaz A. I., Terlevich E., Edmunds, M. G. 1988, *MNRAS*, 235, 633
- Westera P., Lejeune T., Buser R., Cuisinier F., Bruzual G. 2002, *A&A*, 381, 524
- Yoon S.-., Cantiello M., 2010, *ApJ*, 717L, 62Y
- Zurita, A., Beckman, J. E., Rozas, M., Ryder, S. 2002, *A&A*, 386, 801

This paper has been typeset from a \TeX / \LaTeX file prepared by the author.